

Supporting information

Heterostructure conductive interface and melt-penetration-bonding process to enable all-solid-state Li-FeF₃ garnet batteries with high cathode loading

Hailong Wu^{1,2,3,§}, Jiulin Hu^{1,2,3,§}, Songlin Yu^{1,2}, Chilin Li^{1,2,3*}

1 State Key Laboratory of High Performance Ceramics and Superfine Microstructure, Shanghai Institute of Ceramics, Chinese Academy of Sciences, 585 He Shuo Road, 201899 Shanghai, China.

2 Center of Materials Science and Optoelectronics Engineering, University of Chinese Academy of Sciences, 100049 Beijing, China.

3 CAS Key Laboratory of Materials for Energy Conversion, Shanghai Institute of Ceramics, Chinese Academy of Sciences, Shanghai 201899, China.

* The corresponding author. Email: chilinli@mail.sic.ac.cn

§ These authors contribute equally to this work.

Experimental section

Material synthesis.

Li_{6.5}La₃Zr_{1.5}T_{0.5}O₁₂ pellet (LLZTO) was prepared by conventional solid-state reaction reported in our previous work. Specifically, Li₂CO₃, ZrO₂, La₂O₃, and Ta₂O₅ materials (Shanghai Aladdin Bio-Chem Technology Co., Ltd) with a specific molar ratio were employed as precursors to prepare the garnet LLZTO. In order to offset the volatile loss of lithium during the sintering process, a 15% excess of Li₂CO₃ was added. Prior to sintering, the La₂O₃ powder was calcined at 900 °C for 12 h to remove any crystal water. The precursor materials were then mixed together with absolute ethyl alcohol and ball-milled for 12 h at 230 rpm. The resulting dry powder was sintered at 900 °C for 12 h to achieve tetragonal LLZTO. The tetragonal garnet obtained in the preceding step was fragmented and ball-milled for 24 h. Thereafter,

the dry powder was compressed into pellets and sintered at 1250 °C for one hour and 1150 °C for six hours, thereby yielding the final cubic garnet electrolyte. The LLZTO pellet was roughly polished by sandpaper to a thickness of ~ 500 μm, and was then sonicated in an ethanol solution for 30 seconds to wash away any residual powder impurities on surface. After that the pellets were dried by hair dryer and quickly transferred to the glove box in order to minimize the air exposure to form Li₂CO₃ layer. The surface area and thickness of ceramic pellets were fixed at about 0.5 cm² and 0.05 cm, respectively. The relative density of used pellets measured by the Archimedes' principle is ~95%.

The Li₂MoF₆-Cu/Li₂NbF₆-Cu were prepared by solid-state reaction. LiF, molybdenum (Mo)/niobium (Nb), and CuF₂ (Shanghai Aladdin Bio-Chem Technology Co., Ltd) with a molar proportion of 2:1:2 were placed in an alumina crucible after thorough grinding and homogenization. Subsequently, the mixture was subjected to a thermal treatment at 450 °C for a period of 12 h in a tube furnace under nitrogen protection. Then the black powders of Li₂MoF₆-Cu/Li₂NbF₆-Cu were obtained for further use.

Preparation of Li₂MoF₆-Cu modification layer and cell fabrication.

An Li₂MoF₆-Cu layer was prepared by using scalpel to evenly scrape the Li₂MoF₆-Cu powder onto the surface of LLZTO pellet. This procedure was performed under normal air atmosphere. The batteries for performance evaluation were assembled with Li foil anode and specialized cathode. Before assembling the symmetric and full cells, lithium metal was cut into the small discs with a 5 mm diameter and was melted on the surface of garnet with or without interface modification at 230 °C for 30 min. Generally, the cathode was composed of FeF₃ or LiNi_{0.8}Co_{0.1}Mn_{0.1}O₂ (NCM811) powder (Hefei Kejing Inc., China, 100 mg), Super P carbon black (TeenSky Inc., China, 60 mg), polyethylene oxide (PEO) (average Mv: ~2000,000, Aladdin, 246 mg) and bistrifluoromethanesulfonimide lithium salt (LiTFSI) (Sigma-Aldrich, 80 mg). FeF₃ active material was prepared by a deep-eutectic solvent method according to our previous report. The cathode composite was added into anhydrous acetonitrile and

then coated on the carbon-coated aluminum foil. Subsequently, the acetonitrile solvent was removed at 50 °C under vacuum, and the electrode was punched with a diameter of 5 mm. By adjusting the amount of solvent and casting process, the mass loading of FeF₃ or NMC811 cathode ranges from 6 to 8 mg/cm². All the cells were assembled in CR2032-type coin cells in argon filled glove box (content of H₂O, O₂ < 0.1 ppm). It is noted that all the lithium metal full cells were pre-treated at 80 °C for 12 h to facilitate the better integration of electrode/electrolyte interface, especially for the cathode side. The preparation of Li₂NbF₆-Cu modification layer and corresponding cell fabrication are the same as those for Li₂MoF₆-Cu layer.

Electrochemical measurement.

Electrochemical impedance spectra (EIS) of Li symmetric cells were measured by Solartron electrochemical workstation (1260-1296) with frequency range from 0.1 Hz to 10 MHz under a polarization voltage of 5 mV at room temperature or 60 °C. In situ galvanostatic electrochemical impedance spectra (GEIS) of all-solid-state FeF₃/Li cell were tested at 0.1 C rate with an intermittent EIS test at 1 h intervals. The critical current density (CCD) value of Li/Li symmetric cell was determined under an initial current density of 0.1 mA/cm² with an increasing step of 0.1 mA/cm², carrying Li plating and stripping of 0.1 mAh/cm² for each cycle. The galvanostatic cycling test of Li symmetric cell was measured at a current density of 0.2 or 0.5 mA/cm² with a capacity of 0.2 or 0.5 mAh/cm². The Li diffusion coefficient (D_{Li}) for interface modified garnet was estimated also based on Li/Li symmetric cell, where different current densities were applied to make sure that the Li electrode is depleted at one side and deposited on the other side completely. The all-solid-state full cells were tested between 1.2 and 3.9 V for FeF₃ cathode system, between 3.0 and 4.2 V for NCM811 cathode system, and between 2.0 and 4.0 V for LiFePO₄ cathode system at 60 °C. The current density or rate setting is based on the theoretic specific capacities of FeF₃ (1C = 712 mA/g), NCM811 (1C = 280 mA/g) and LiFePO₄ (1C = 170 mA/g), respectively. The galvanostatic intermittent titration technique (GITT) was employed to evaluate the Li diffusion coefficient (D_{Li}) of cathode material in the garnet all-

solid-state system. The all-solid-state FeF₃/Li cell was repeatedly charged and discharged at 0.1 C rate for 15 min followed by a relaxation process for 4 h to obtain the GITT curves. All the assembled coin cells were tested on a LAND-CT2001A Battery Test System after heat treatment at 80 °C for 12 h to construct the intimate contact between cathode and garnet electrolyte. A Tafel analysis was conducted on the all-solid-state FeF₃/Li cells, with a scan rate of 1 mV/s at the regions of intercalation and conversion plateaus with the holding of plateau potentials (i.e., 3.0 and 2.0 V, respectively) for 1 h. The Tafel test was conducted on VersaSTAT electrochemical workstation. The Li⁺ transference number (t_{Li^+}) values of pure and Li₂MoF₆-Cu modified LLZTO are evaluated by chronoamperometry and EIS techniques. The t_{Li^+} values are estimated according to the Bruce-Vincent method:

$$t_{Li^+} = \frac{I_s(\Delta V - I_0 R_0)}{I_0(\Delta V - I_{ss} R_{ss})}$$

In this equation, I_0 and I_s represent the currents at the initial or stabilized states respectively, R_0 and R_{ss} represent the interfacial resistances at the initial or stabilized states respectively, and ΔV is a constant voltage (10 mV) applied across the bulk electrolyte.

DRT analysis.

DRT (distribution of relaxation time) technology is a model-free analysis of impedance evolution, and it is transformed from the Nyquist plots of EIS results based on frequency domain according to the following equation.

$$Z(\omega) = R_\infty + \int_0^\infty \frac{\gamma(\tau)}{1 + j\omega\tau} d\tau$$

The DRT was conducted to calculate the distribution function $\gamma(\tau)$ of characteristic time constant based on EIS data, and then to obtain the kinetic information of electrochemical system according to the analysis of $\gamma(\tau)$. The DRT analysis was conducted by Python according to the GP-DRT model developed by Ciucci's research team (*Electrochimica Acta*, 2020, **331**, 135316). Regularization and Gaussian process (GP) were implied to optimize the ill-posed problem, which is particularly sensitive to experimental error.

Theoretical calculation.

Density functional theory (DFT) was used when the structure relaxation and electronic structure calculation were conducted within the DMol3 module in Materials Studio. The projector augmented wave method and the semilocal Perdew-Burke-Ernzerh of exchange-correlation functions were adopted in the present calculations. An all-electron double numerical basis set with polarization functions (DNP basis set) was used during calculation. The convergence tolerance quality of geometry optimization was set as 1.0×10^{-5} au for energy, 1.0×10^{-4} au/Å for maximum force, and 1.0×10^{-4} Å for maximum displacement. The self-consistent field (SCF) tolerance was set to 1.0×10^{-6} au. The structures with LiF (200), Cu (111) and Mo (110) surfaces were constructed. The LiF@Cu and LiF@Mo heterojunctions were constructed by LiF (200) with Cu (111) and Mo (110), respectively.

Materials Characterization.

The crystal structure and crystallinity of obtained $\text{Li}_2\text{MoF}_6\text{-Cu}$ and $\text{Li}_2\text{NbF}_6\text{-Cu}$ powders were identified using an X-ray powder diffractometer (XRD, Bruker, D8 Discover) with Cu-K α radiation. The morphology and elemental distribution of obtained $\text{Li}_2\text{MoF}_6\text{-Cu}$ powder, as well as cross-sectional morphology and elemental distribution of Li/garnet interface after lithiation and cycling were detected by scanning electron microscopy (SEM, Magellan 400 L, FEI) and energy-dispersive X-ray spectroscopy (EDS). The cross-sectional morphology of cathode/garnet interface after hot melt-penetration-bonding process and cycling was also detected by SEM imaging. A transmission electron microscopy (TEM, JEOL JSM-6700F TEM) investigation was conducted to examine the morphology and structure of lithiated and cycled $\text{Li}_2\text{MoF}_6\text{-Cu}$ layer. The cycled $\text{Li}_2\text{MoF}_6\text{-Cu}$ layer was obtained by scraping off the interface layer after disassembling Li symmetric cell, which had been cycled for 100 h under 0.2 mA/cm² and 0.2 mAh/cm². The electron diffraction patterns were collected with a selected area electron diffraction (SAED) aperture of 10 μm inserted. The components of $\text{Li}_2\text{MoF}_6\text{-Cu}$ layer after lithiation were identified using X-ray

photoelectron spectroscopy (XPS, Thermo scientific ESCALab-250), with an Al-K α anode source.

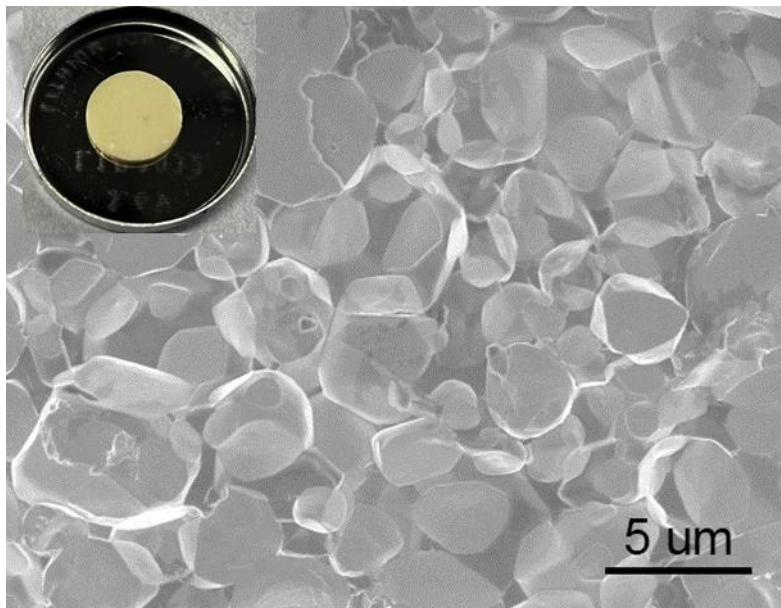


Figure S1. Cross-section SEM image of sintered garnet electrolyte, showing no substantial Li₂CO₃ coverage, inset: digital image of prepared LLZTO.

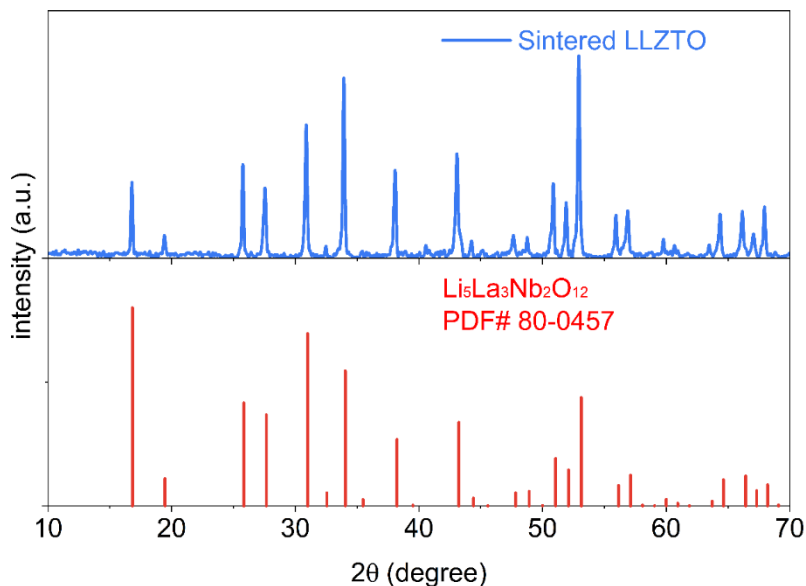


Figure S2. XRD pattern of sintered LLZTO pellet. XRD demonstrates that the sintered fresh sample has a cubic crystal structure of garnet phase according to the pattern of Li₅La₃Nb₂O₁₂ (PDF#80-0457).

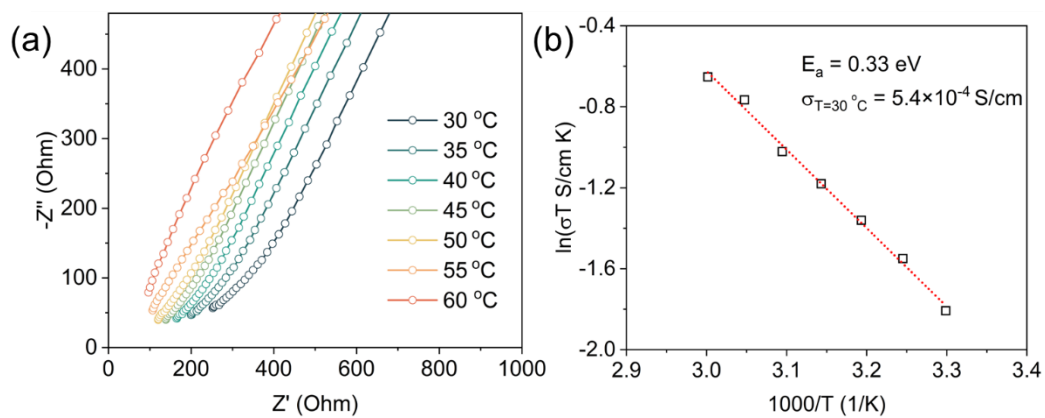


Figure S3. (a) Nyquist plots of Ag/LLZTO/Ag structure from 30 °C to 60 °C. (b) Corresponding Arrhenius plots for calculation of activation energy (E_a).



Figure S4. Optical photographs of raw materials and obtained product.

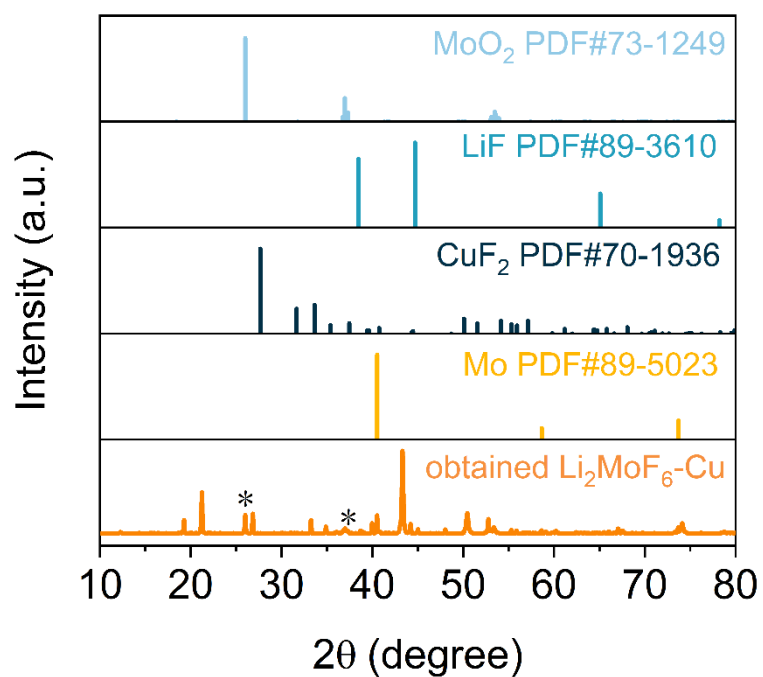


Figure S5. XRD pattern of Li₂MoF₆-Cu sample synthesized at 450 °C for 12 h under nitrogen protection. Comparison with XRD standard card library reveals that no raw material is discovered, and only a small quantity of molybdenum oxide is detected.

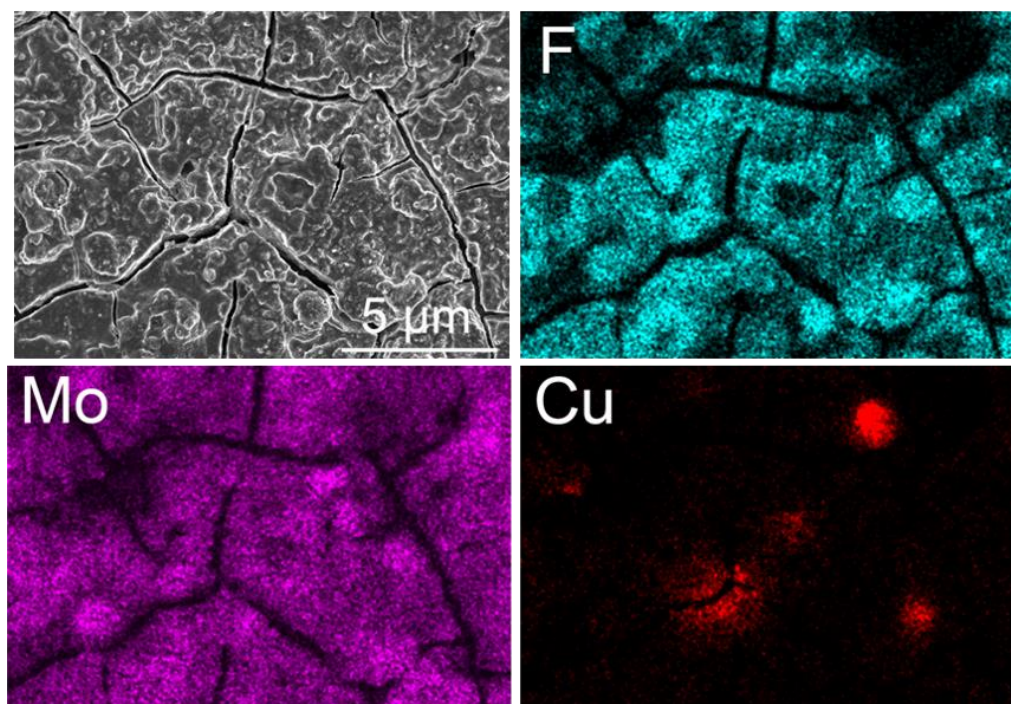


Figure S6. SEM image of $\text{Li}_2\text{MoF}_6\text{-Cu}$ layer and corresponding EDS mapping results of F, Mo and Cu elements.

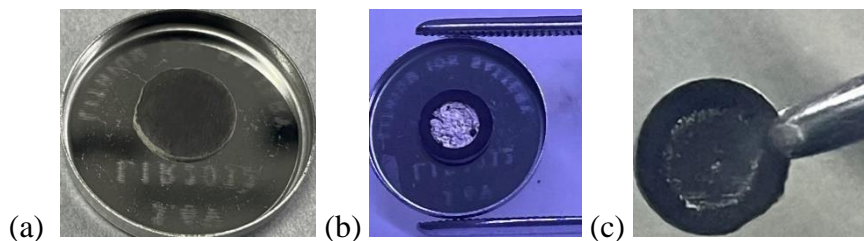


Figure S7. Optical images of (a) $\text{Li}_2\text{MoF}_6\text{-Cu}$ coated on LLZTO, (b) lithiation of $\text{Li}_2\text{MoF}_6\text{-Cu@LLZTO}$ after melting lithium at 230 °C for 30 min, (c) $\text{Li}_2\text{MoF}_6\text{-Cu@LLZTO}$ after tearing off surface-fused lithium.

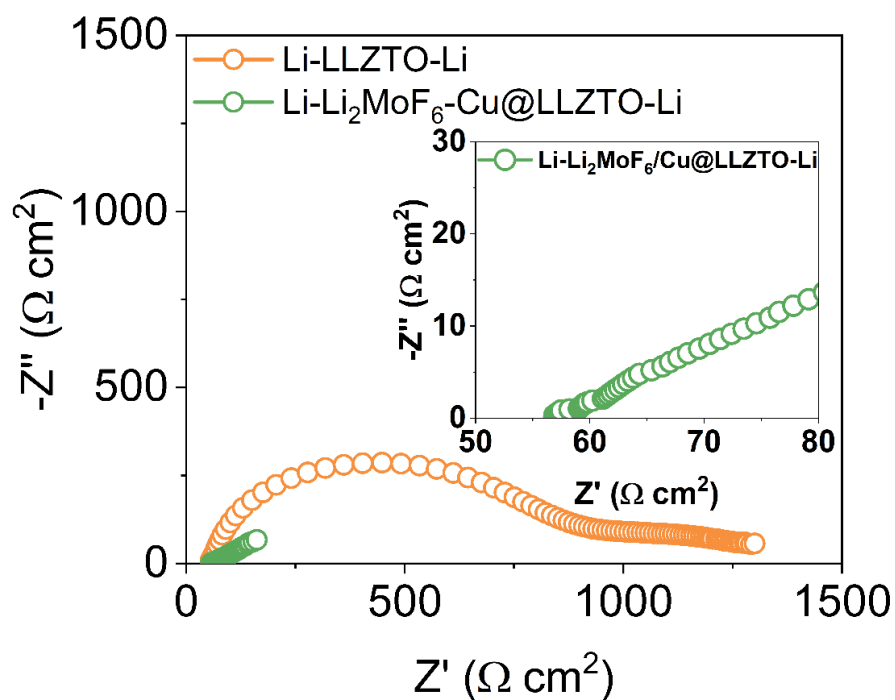


Figure S8. Nyquist plots of symmetric Li-LLZTO-Li and $\text{Li-Li}_2\text{MoF}_6\text{-Cu@LLZTO-Li}$ symmetric cells tested at 60 °C, inset: enlarged Nyquist plots of $\text{Li-Li}_2\text{MoF}_6\text{-Cu@LLZTO-Li}$ all-solid-state symmetric cell.

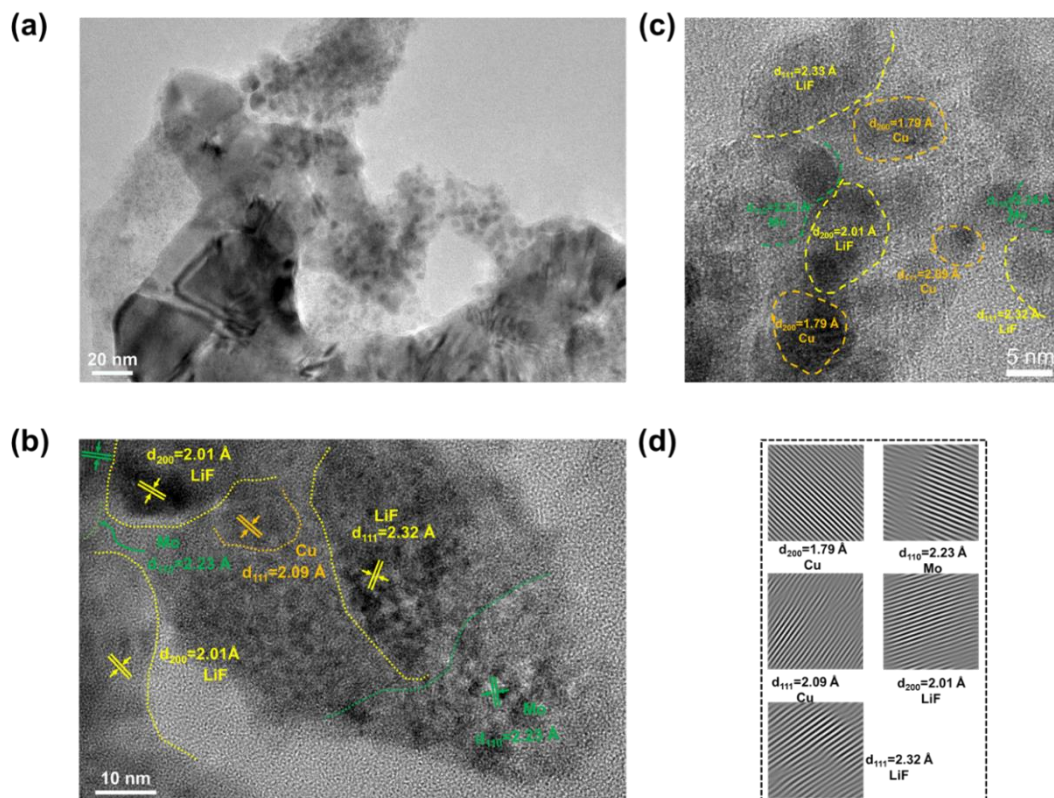


Figure S9. (a) TEM image of MIEC layer in Li-Li₂MoF₆-Cu@LLZTO interface after cycling for 100 h. (b,c) HRTEM images of corresponding MIEC layer in different scales. (d) Corresponding inverse Fourier transform patterns of product phases found in (c).

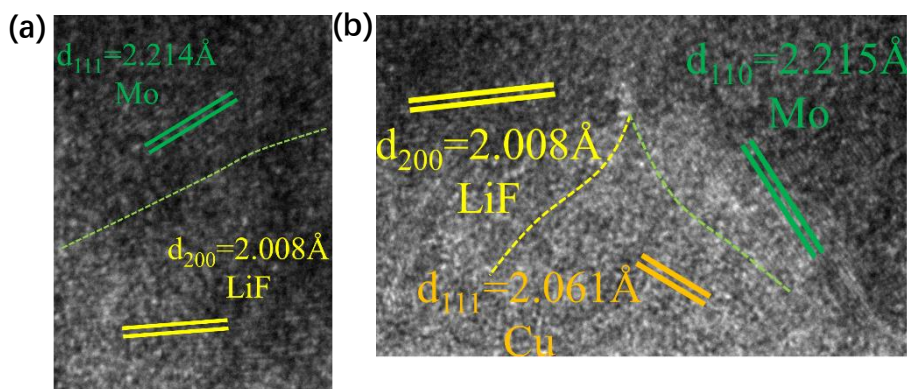


Figure S10. Enlarged TEM images with heterojunctions corresponding to Figure 3b

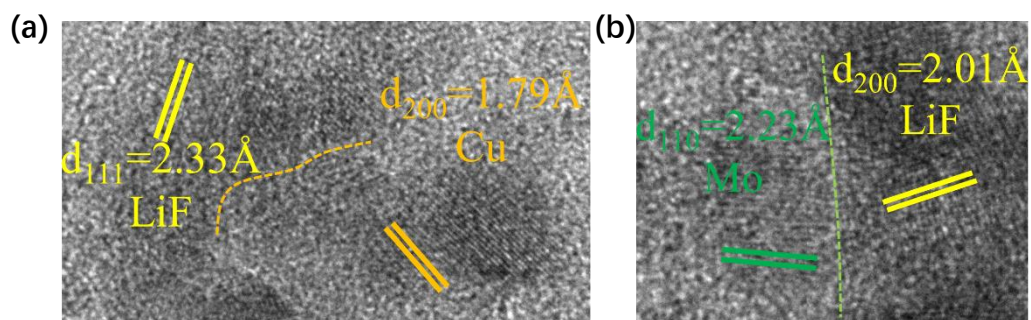


Figure S11. Enlarged TEM images with heterojunctions corresponding to Figure S9C

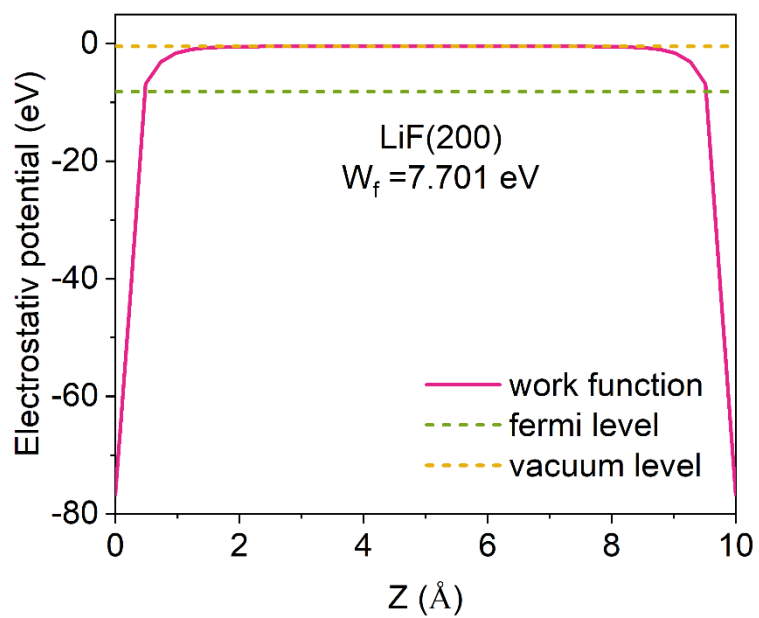


Figure S12. Electrostatic potential profile of LiF (200) plane.

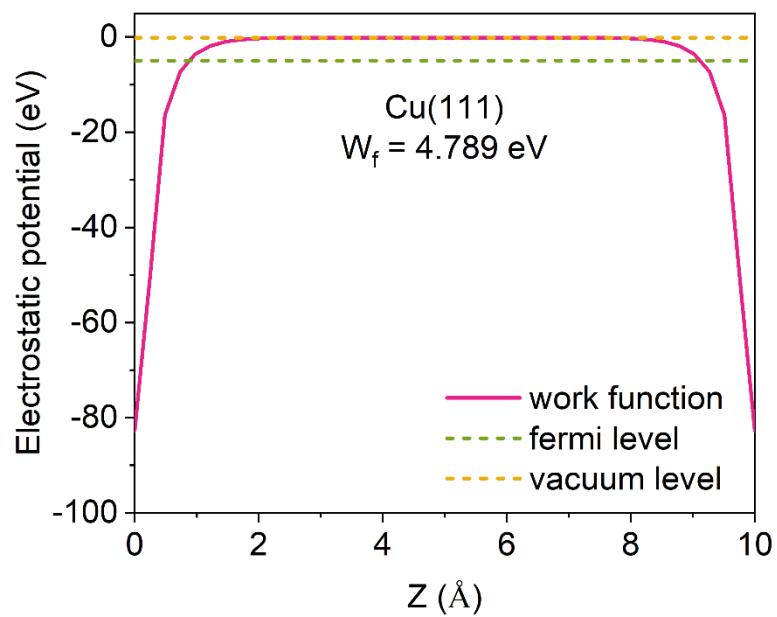


Figure S13. Electrostatic potential profile of Cu (111) plane.

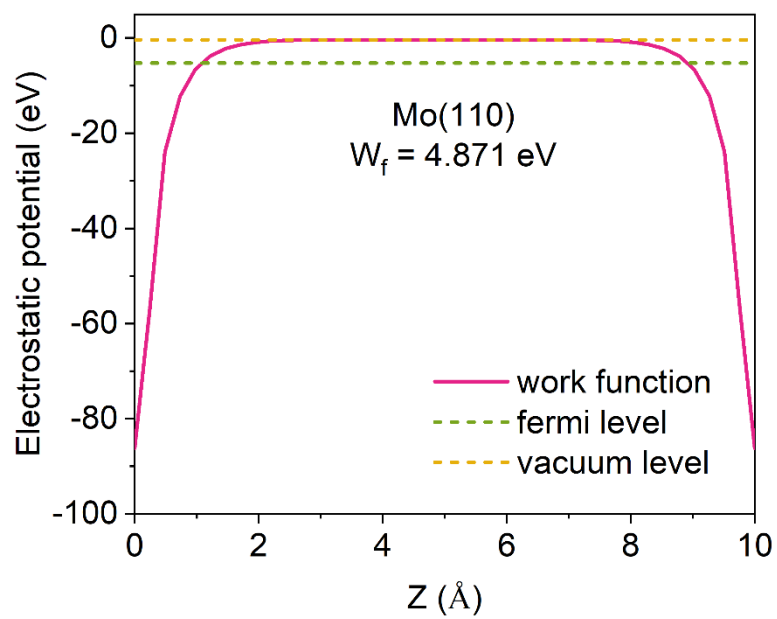


Figure S14. Electrostatic potential profile of Mo (110) plane.

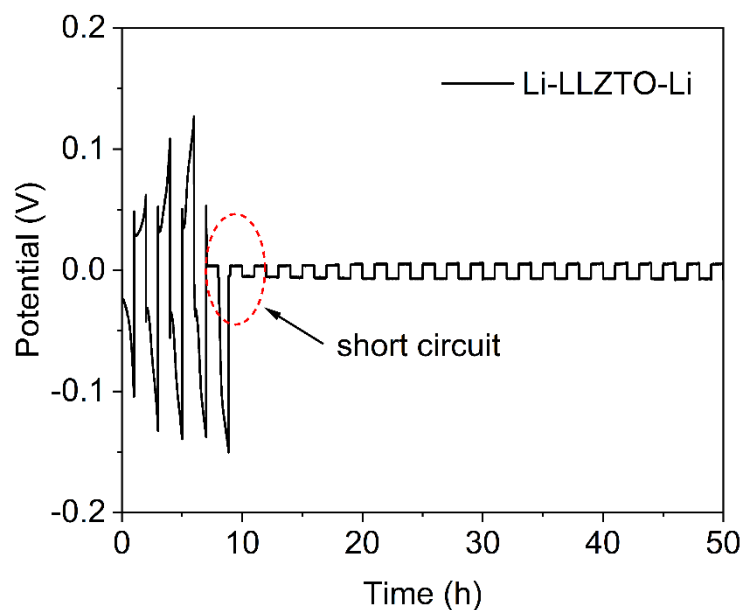


Figure S15. Cycling performance of Li-LLZTO-Li symmetrical cell at 0.2 mA/cm^2 with a capacity of 0.1 mAh/cm^2 at $60 \text{ }^\circ\text{C}$, pretested with a gradual increased current density from 0.05 mA/cm^2 to 0.2 mA/cm^2 in a step of 0.05 mA/cm^2 with a 2 h resting interval.

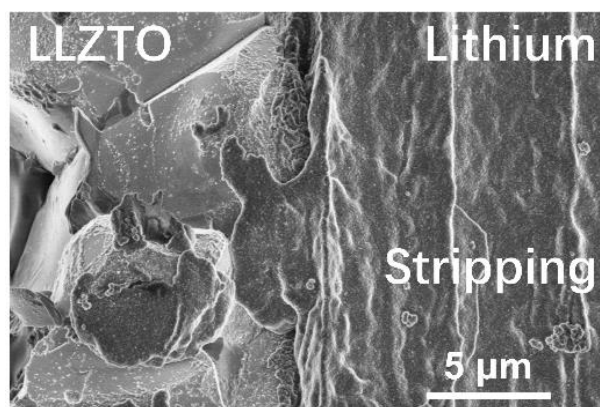


Figure S16. Cross-section SEM image of interface between Li and $\text{Li}_2\text{MoF}_6\text{-Cu@LLZTO}$ after stripping based on an area capacity of 0.4 mAh/cm^2 .

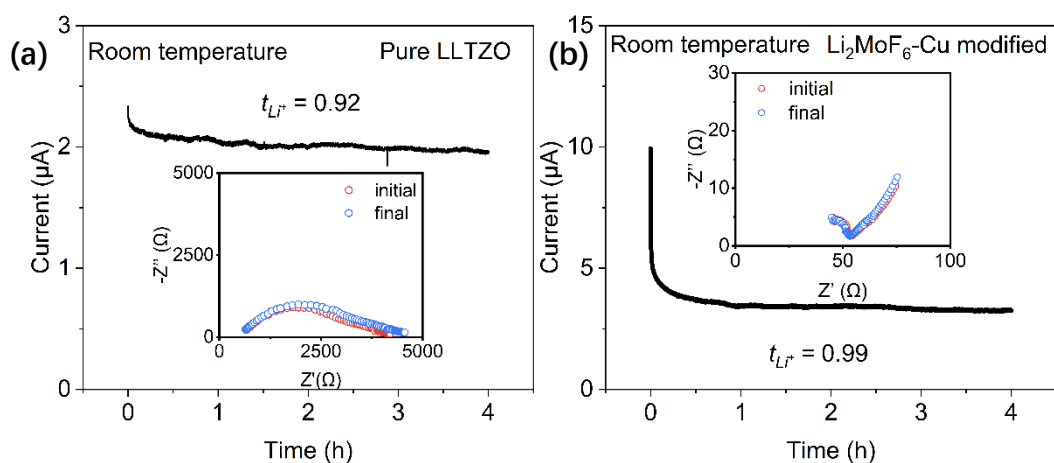


Figure S17. Current-time curves of (a) Li-LLZTO-Li and (b) Li- $\text{Li}_2\text{MoF}_6\text{-Cu}$ @LLZTO-Li cells under a DC polarization of 10 mV. The insets illustrate the EIS plots before and after polarization.

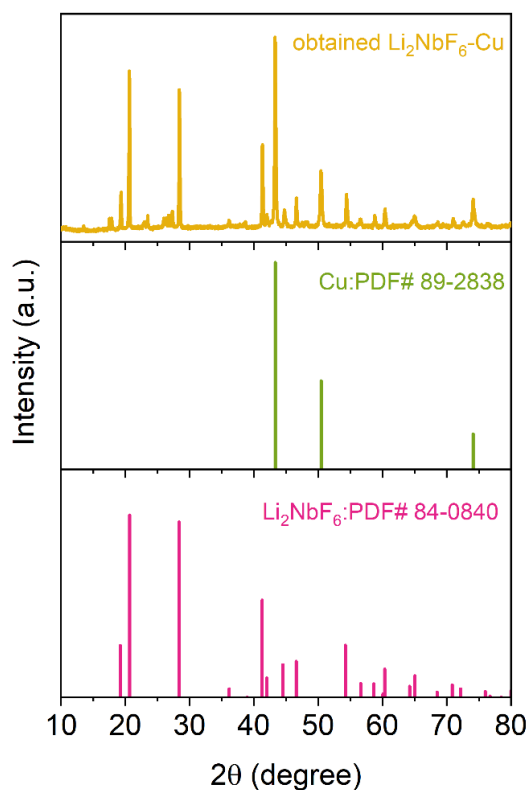


Figure S18. X-ray diffraction pattern of $\text{Li}_2\text{NbF}_6\text{-Cu}$ sample synthesized at 450 $^\circ\text{C}$ for 12 h under nitrogen protection.

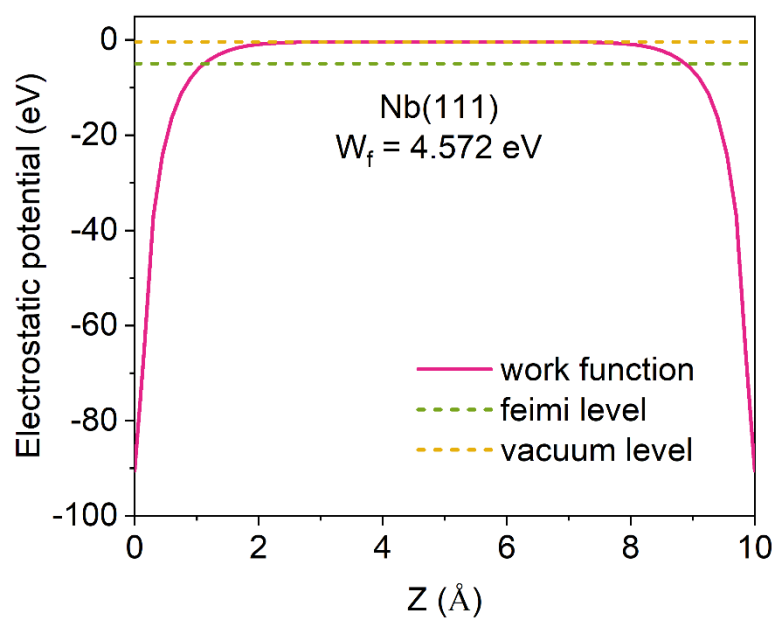


Figure S19. Electrostatic potential profile of Nb (111) plane.

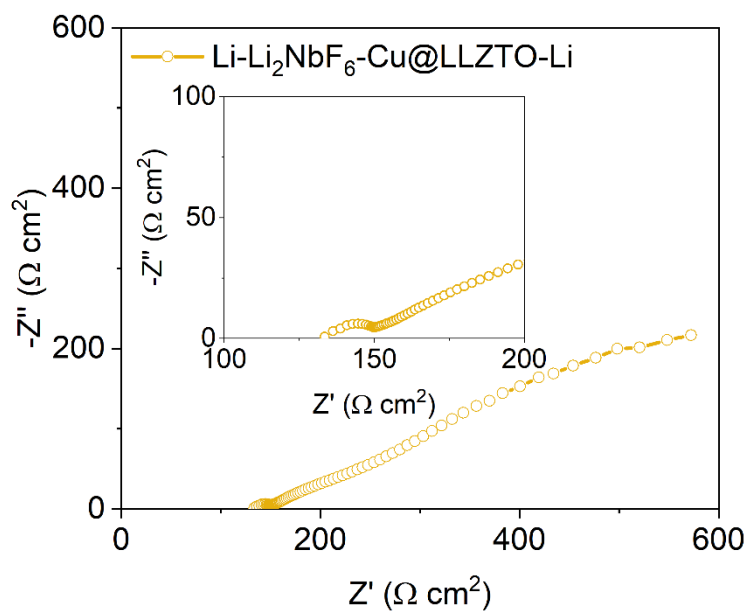


Figure S20. Nyquist plots of Li-Li₂NbF₆-Cu@LLZTO-Li all-solid-state symmetric cell tested at 60 °C, inset: enlarged Nyquist plots of this symmetric cell.

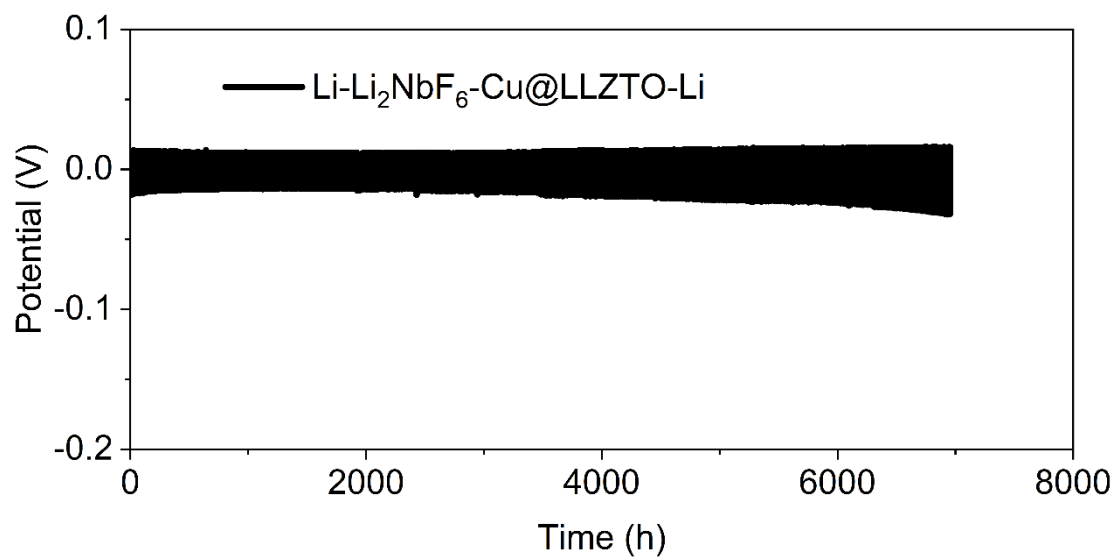


Figure S21. Cycling performance and voltage profiles of Li-Li₂NbF₆-Cu@LLZTO-Li symmetrical cell at 0.2 mA/cm² with a capacity of 0.2 mAh/cm².

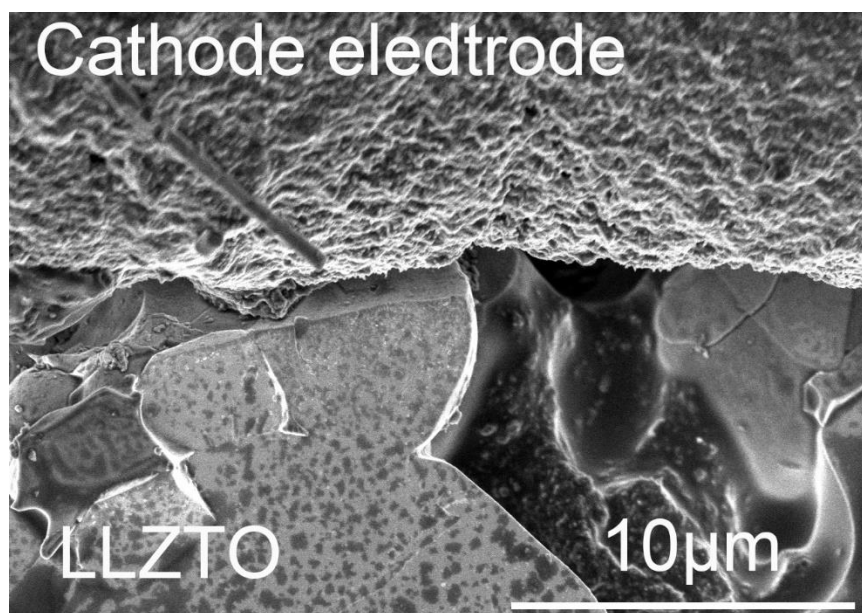


Figure S22. Cross-sectional SEM image of initial FeF₃/LLZTO interface after heating for 12 h.

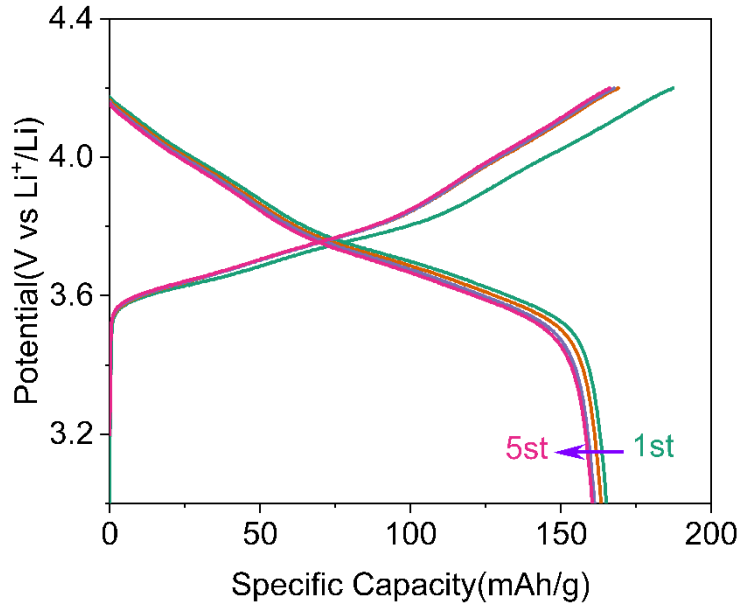


Figure S23. Charge and discharge curves of NCM811|Li₂MoF₆-Cu@LLZTO|Li full cell with high cathode loading of 8 mg/cm² at 0.1 C under 60 °C.

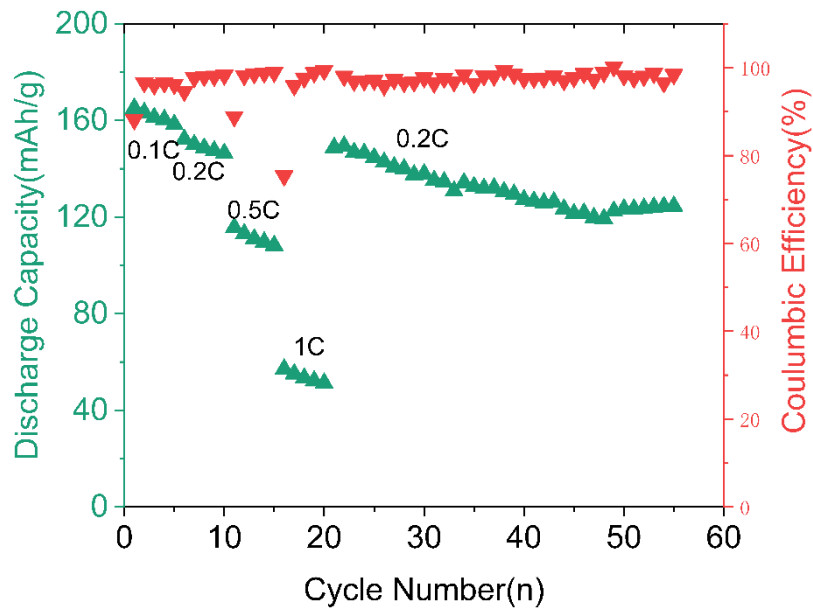


Figure S24. Rate performances of NCM811|Li₂MoF₆-Cu@LLZTO|Li full cell with high cathode loading of 8 mg/cm² under 60 °C.

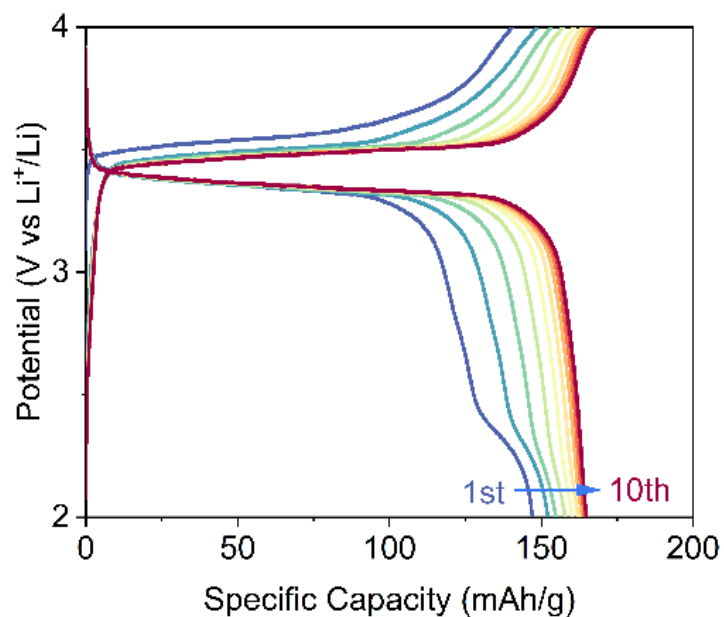


Figure S25. Charge and discharge curves of LFP|Li₂MoF₆-Cu@LLZTO|Li full cell with high cathode loading of 8 mg/cm² at 0.1 C (1C = 170 mA/g) under 60 °C..

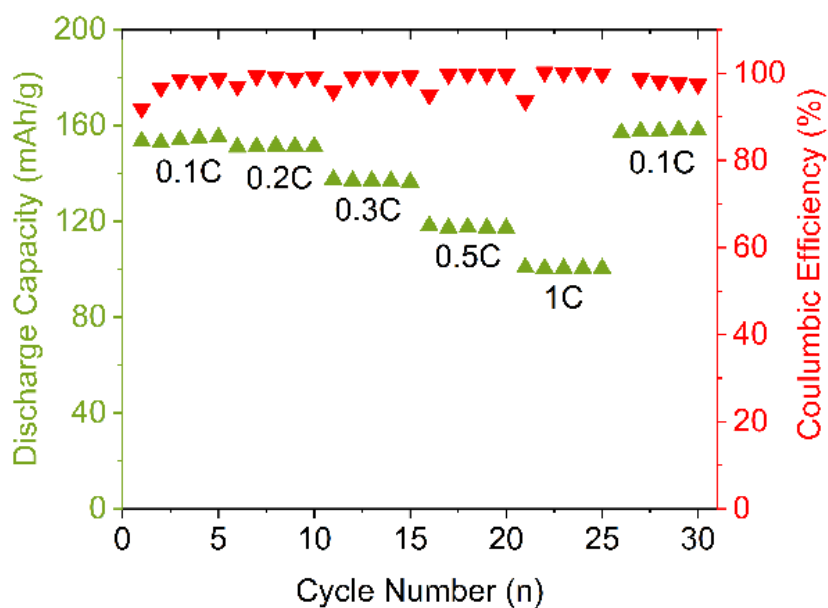


Figure S26. Rate performance of LFP|Li₂MoF₆-Cu@LLZTO|Li full cell with high cathode loading of 8 mg/cm² under 60 °C..

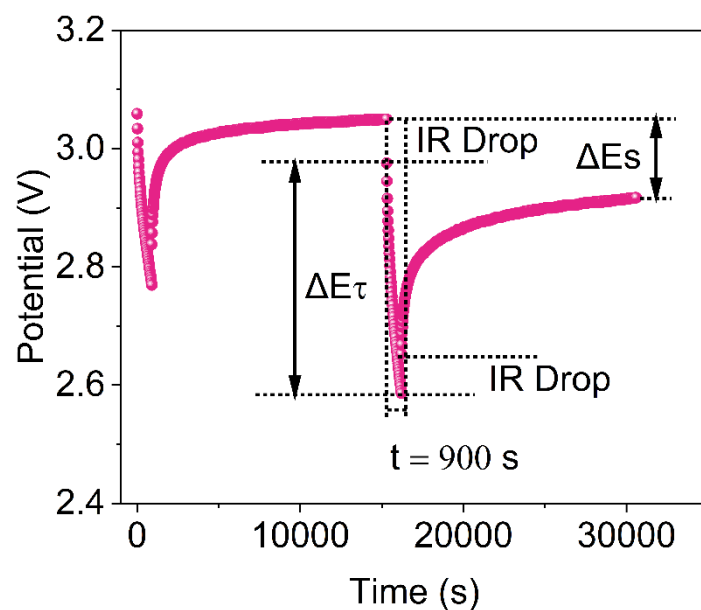


Figure S27. Voltage profiles for a single step of GITT of $\text{FeF}_3|\text{Li}_2\text{MoF}_6\text{-Cu@LLZTO}|\text{Li}$ full cell at ~ 3.1 V during discharging.

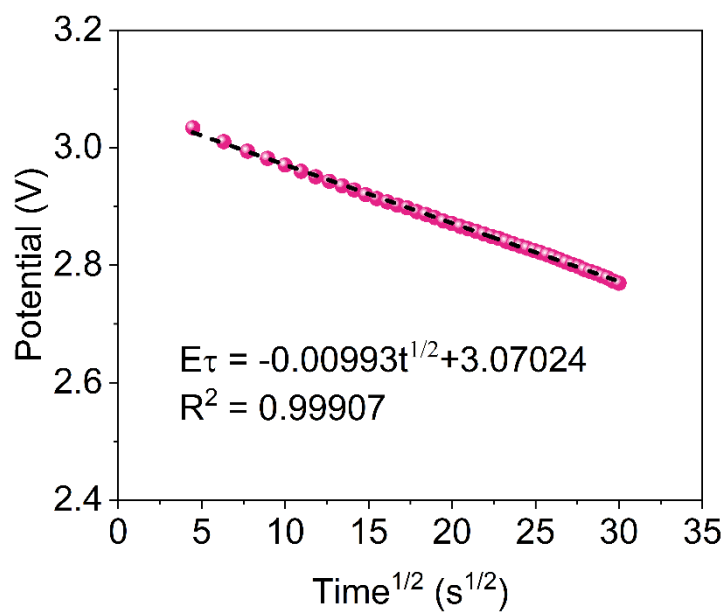


Figure S28. Representation of transient voltage as a function of the square root of titration time according to Figure S21.

Table S1. Li adsorption energies for LiF, Cu, Mo and Li metal substrates.

Substrate	Adsorption energy (eV)
Li (100)	-0.847
Li (110)	-1.852
Li (111)	-2.496
Cu (100)	-1.024
Cu (110)	-1.344
Cu (111)	-0.8
Mo(100)	-1.507
Mo(110)	-1.229
Mo(111)	-2.173
LiF(001)	-0.106
LiF(200)	-0.104